AUCTORES
Globalize your Research

Journal of Clinical Research and Reports

Song Chol Kim *

Open Access

Research Article

Analysis of Fluid Flow Characteristics for Stress-Sensitivity Dual-Porosity Reservoir considering Elastic Outer Boundary

Song Guk Han, Song Chol Kim *

Faculty of Earth Science and Technology, Kim Chaek University of Technology, Pyongyang, Democratic People's Republic of Korea.

***Corresponding Author:** Song Chol Kim, Faculty of Earth Science and Technology, Kim Chaek University of Technology, Pyongyang, Democratic People's Republic of Korea.

Received date: September 12, 2024; Accepted date: November 01, 2024; Published date: November 09, 2024

Citation: Song Guk Han, Song C. Kim, (2024), Analysis of Fluid Flow Characteristics for Stress-Sensitivity Dual-Porosity Reservoir considering Elastic Outer Boundary, *J Clinical Research and Reports*, 16(1); **DOI:10.31579/2690-1919/406**

Abstract

Previous researchers have considered the influence of stress sensitivity and elastic outer boundary on the flow characteristics of fluids in reservoir, and solved the problem by considering stress sensitivity and elastic outer boundary conditions when analyzing the flow characteristics, but the stress sensitivity and elastic outer boundary conditions are not taken into account at the same time, the error still arises in the well test analysis.

In order to simplify the complex problem in solving the model, we obtained analytical solutions in Laplace space by applying inverse transformation and obtained the pressure and pressure derivative curve, and analyzed the sensitivity of the characteristic values for pressure and pressure derivative curve.

In order to simplify the complex problem in solving the model, Pedrosa's transformation and perturbation's transformation were applied.

Using these transformations, the nonlinear partial differential equation was linearly transformed. By Laplace transformation, we obtained analytical solutions in Laplace space and applied inverse transformation to obtain solutions in real space, and plotted the pressure and pressure derivative curves.

The model accuracy was verified by comparison with previous studies and sensitivity analysis of the characteristics for pressure and pressure derivative curves was performed.

This study is of great significance in improving the accuracy of the parameters of the well and reservoir determined by well test analysis.

Keywords: stress sensitivity; dual-porosity reservoir; well testing; elastic outer boundary

Introduction

During oil extraction, the permeability of the reservoir changes due to the decrease of the pressure of reservoir and the increase of effective stress. Many researchers have studied reservoir models considering the stress sensitivity and stress sensitivity of reservoir.

Jiang and Yang (2018) presented a complete coupled model of fluid flow and geomechanics characterizing stress-sensitive reservoir in hydraulic fractured coal bed methane reservoirs, and Guo etc. (2015) presented pressure unsteady analysis and flow attenuation analysis for hydraulic fracturing vertical wells with finite conductivity in shale reservoirs considering multi-flow mechanisms including desorption, diffusion, Darcy flow and stress sensitivity.

Zhao etc. (2020), Jabbari etc. (2012) studied the effect of stress sensitivity on analyzing the flow characteristics of fluids in fractured reservoirs, Wang and Wang (2016) proposed that the effect of stress sensitivity on establishing a semi-analytical model considering the sliding effect in fractured gas reservoirs, Huang etc. (2018a) presented an unsteady flow model of horizontal well in stress sensitive composite reservoirs, Li etc. (2017) developed a dual-porosity medium model of horizontal well considering the influence of stress sensitivity.

Aguilera (2008) proposed a material balance equation considering the effective compressibility of the dual-porous medium, Wang etc. (2014; 2017c) and Luo etc. (2021) and Mo etc. (2016) considered the stress sensitivity when establishing a fluid flow model in a fractured reservoirs.

Ren and Guo (2018) studied the general analytical method of unsteady flow rate considering the influence of stress sensitive permeability, Jelmert and Toverud (2017) presented a model of stress sensitive reservoir and their solution based on the outer elastic modulus and plotted the corresponding typical curve.

Li etc. (2020a) proposed a sampling model that considers stress sensitivity based on the combination of fluid flow characteristics and rock mechanics in triple porous media including kerogen, inorganic and fracture networks.

Chen etc. (2021) developed a model considering the threshold pressure gradient, gas slip and stress sensitivity when developing a mathematical model in a dual-porosity gas reservoir, and Xue etc. (2021) conducted a study of a dense sandstone gas reservoir where water is taken together and found that the influence of stress sensitivity in a dense sandstone gas reservoir is strongly influenced.

Lian etc. (2011) and Zhao etc. (2013) studied the stress sensitivity of permeability in the laboratory, Wang etc. (2018), Shu and Yan (2008), Selvadurai etc. (2018), Wang etc. (2018), Wang etc. (2011), Feng etc. (2021), Tian etc. (2015) conducted a laboratory study on the effect of stress sensitivity on the bed gas layer, and Zheng etc. (2015) conducted experiments using nuclear magnetic resonance technique to investigate the relationship between the permeability and its effective stress, and Zhang etc. (2019) proposed the influence of stress sensitivity on a gas reservoir, and Zhang etc. (2019) proposed the influence of stress sensitivity on the system.

Shovkun and Espinoza (2017) considered the flow of fluid taking into account the stress induced by adsorption in the stress-sensitive coal bed methane, and carried out geomechanical simulations considering shear rupture in the coal reservoir and migration of coal dust. Wu etc. (2018c) and Xu etc. (2021) proposed a well test model in a multi-hydraulic fractured horizontal well considering stress sensitivity.

Zhang etc. (2010) developed an analytical well test model considering stress sensitivity to several factors in a low permeability reservoir, and Wang etc. (2017a) considered the effect of stress sensitivity on horizontal well test analysis in a multi-view low permeability natural fracture reservoirs.

Wu etc. (2018b) and Ji etc. (2017), Huang etc. (2018b) considered stress sensitivity in a dense reservoir, Wu etc. (2018a) proposed a multi-hydraulic fractured horizontal well test model considering stress sensitivity in a dense gas reservoir, Wang etc. (2020), Liu etc. (2015), Du etc. (2020), proposed a mathematical model considering stress sensitivity in a vertical well of a hydraulic fractured coal reservoir, Chen etc. (2016), Wang etc. (2021) proposed a numerical model considering stress sensitivity in a vertical well of a hydraulic fractured coal reservoir , and Wang etc. (2021) conducted a study.

Cao etc. (2021) and Yan etc. (2021) conducted an unsteady filtration study considering the effect of sand extraction on filtration and stress sensitivity in a well where sand is taken together.

Zhang and Tong (2008) investigated the unsteady pressure response of the purge medium in stress-sensitive reservoirs.

Gao etc. (2021) proposed a well-testing model considering stress sensitivity when performing pressure recovery tests in a high-pressure complex gas reservoir at the depth.

So far, as all idealized outer boundaries related to the stress sensitivity considered by the authors are considered, it is considered that there is no strictly idealized boundary in the reservoirs, and is extremely rare, therefore, considering the external boundary as idealized boundaries, the reservoir cannot be objectively described and the error can be avoided in the analysis.

Several researchers have investigated the flow characteristics in reservoir by considering the elastic outer boundary.

Li etc. (2019a) considered the outer boundary as an elastic boundary in the filtration modeling of homogeneous reservoir, Li etc. (2020b) modeled the extended Bessel equation by introducing elastic boundary value condition, proposed the elastic boundary value problem, and proposed the filtering model of the loose homogeneous reservoir under elastic outer boundary condition, Kim etc. (2021a) considered the outer boundary condition as an elastic boundary condition, introduced the effective borehole radius, and introduced the effective borehole radius, and Zheng etc. (2021) developed a dual-medium filtration model of the shale gas reservoir with elastic outer boundary considering the adsorption and desorption process.

In the analysis of fluid flow characteristics in reservoir, both stress sensitivity and elastic outer boundary conditions have a significant effect, but previous studies have not considered this simultaneously.

In this paper, a well test analysis model of a dual-porosity reservoir considering stress sensitivity and elastic outer boundary conditions simultaneously is developed and the solution is obtained.

EOB condition

Li et al. (2019a) defined an elastic coefficient of reservoir as follows:

$$\varepsilon_r^P = \varepsilon_r^P(r,t) = \frac{\partial \ln P}{\partial \ln r} = \frac{r}{P}\frac{\partial P}{\partial r} \quad (1)$$

$$P = p_i - p\,, \quad (2)$$

where is the rate of the relative change of the pressure difference P with respect to r

p is the function of time (t) and position (x, y, z).

$$p = p(x,y,z,t)\,, \quad (3)$$

As shown in Figure.1, the farther the distance from a well is, the lower the pressure difference is. Thus, the change direction of pressure difference is opposite to the change direction of the position.

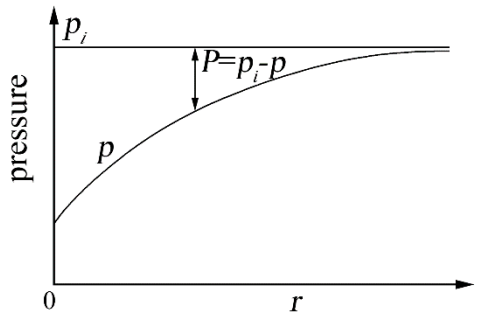

Figure 1: Distribution of pressure in reservoir versus radius, r

Therefore, the elastic coefficient of outer boundary in a cylinder reservoir can be defined as follows (Kim et al., 2021a):.

$$\varepsilon_\Gamma^P = \varepsilon_\Gamma^{P_D} = \varepsilon_R^{P_D} = \varepsilon_{R_D}^{P_D} = -\left.\frac{\partial \ln P}{\partial \ln r}\right|_{r=R} = -\left.\frac{\partial \ln P_D}{\partial \ln r_D}\right|_{r_D=R_D} \quad (4)$$

From Eq. 4, the EOB condition may be obtained as follows:

$$\left[\varepsilon_\Gamma^P P + r\frac{\partial P}{\partial r}\right]_{r=R} = 0 \quad (5)$$

or

$$\left[\varepsilon_\Gamma^{P_D} P_D + r_D\frac{\partial P_D}{\partial r_D}\right]_{r_D=R_D} = 0 \quad (6)$$

Eq. 5 or 6 is an elastic outer condition.

Methodology

Physical model

1) Reservoir consists of the natural fracture and matrix, the fluid flows through the nature fracture. That is, the reservoir a dual-porosity and a single permeability reservoir.
2) It is a natural fractured reservoir considering stress sensitivity in permeability.
3) The reservoir has a constant thickness h.
4) The fluid flow is assumed to be isotropic and a single phase.
5) The effects of the gravity and capillary are neglected.

Mathematical model

SSP

In order to describe the degree of the SSP of reservoir and its influence, Pedrosa (1986) introduced the concept of a permeability modulus γ for the low-permeability homogenous reservoir. As the reservoir pressure decreases, the opening of natural fracture decreases. Therefore, the permeability of the natural fracture also decreases.

The permeability modulus □□ is defined as follows:

$$\gamma = \frac{1}{k_f}\frac{dk_f}{dp_f}, \tag{7}$$

Integrating Eq. 1,

$$k_f = k_{fi}e^{-\gamma(p_i - p_f)} \tag{8}$$

Continuity equation

$$\frac{1}{r}\frac{\partial(r\rho_f v_f)}{\partial r} = \frac{\partial(\rho_f \phi_f)}{\partial t} - q^* \tag{9}$$

The continuity equation of natural fracture system may be obtained as follows:

$$\frac{1}{r}\frac{\partial(r\rho_m v_m)}{\partial r} = \frac{\partial(\rho_m \phi_m)}{\partial t} + q^* \tag{10}$$

Since the permeability of matrix is extremely low, fluid flow between matrices is negligible and fluid flow from matrices to natural fractures may occur. Therefore, the following equation is obtained.

$$\frac{1}{r}\frac{\partial(r\rho_m v_m)}{\partial r} = 0 \tag{11}$$

Motion equation

It is assumed that the fluid flow in natural fracture system obeys Darcy's law. The following equation may be obtained, which shows the fluid flow in natural fracture.

$$v_f = \frac{k_f}{\mu}\frac{\partial p_f}{\partial r} \tag{12}$$

Substituting Eq. 8 into Eq. 12,

$$v_f = \frac{k_{fi}e^{-\gamma(p_i - p_f)}}{\mu}\frac{\partial p_f}{\partial r} \tag{13}$$

State equation

To describe the changes of oil density in the natural fracture and matrix during production of oil, the following equations are applied, respectively.

$$\rho_f = \rho_o e^{C_o(p_f - p_i)} \tag{14}$$

$$\rho_m = \rho_o e^{C_o(p_m - p_i)} \tag{15}$$

To describe the changes of porosity of the natural fracture and matrix during production of oil, the following equations are applied, respectively.

$$\phi_f = \phi_{fi}e^{C_f(p_f - p_i)} \tag{16}$$

$$\phi_m = \phi_{mi}e^{C_m(p_f - p_i)}, \tag{17}$$

Interporosity flow equation between matrix and fracture

It is assumed that the interporosity flow is pseudo-steady state. Then, the following equation should be satisfied (Warren and Root, 1963):

$$q^* = \frac{\alpha k_m \rho_o}{\mu}(p_m - p_f) \tag{18}$$

Seepage differential equation

In order to obtain a seepage differential equation for matrix system, Eqs. 15, 17 and 18 are substituted into Eq. 10.

$$\frac{\phi_{mi}\mu C_{mt}}{k_{fi}}\frac{\partial p_m}{\partial t} + \frac{\alpha k_m}{k_{fi}}(p_m - p_f) = 0, \tag{19}$$

Eq. 19 is a seepage differential equation for the matrix system in the low-permeability natural fracture reservoir.

In order to obtain a seepage differential equation for natural fracture system, Eqs. 13, 14, 16 and 18 are substituted into 9.

$$\frac{\partial^2 p_f}{\partial r^2} + \frac{1}{r}\frac{\partial p_f}{\partial r} + \gamma\left(\frac{\partial p_f}{\partial r}\right)^2 = e^{-\gamma(p_f - p_i)}\left[\frac{\phi_{fi}\mu C_{ft}}{k_{fi}}\frac{\partial p_f}{\partial t} - \frac{\alpha k_m}{k_{fi}}(p_m - p_f)\right], \tag{20}$$

Substituting Eq. 19 into Eq. 20,

$$\frac{\partial^2 p_f}{\partial r^2} + \frac{1}{r}\frac{\partial p_f}{\partial r} + \gamma\left(\frac{\partial p_f}{\partial r}\right)^2 = e^{-\gamma(p_f - p_i)}\left[\frac{\phi_{fi}\mu C_{ft}}{k_{fi}}\frac{\partial p_f}{\partial t} + \frac{\phi_{mi}\mu C_{mt}}{k_{fhi}}\frac{\partial p_m}{\partial t}\right]. \tag{21}$$

Equation 21 is a seepage differential equation for the natural fracture system considering the SSP in the low-permeability natural fracture reservoir.

Initial and boundary conditions

The reservoir has the uniform pressure. Therefore, initial condition is as follows.

$$p_f(r,t)\big|_{t=0} = p_i, \tag{22}$$

$$p_m(r,t)\big|_{t=0} = p_i. \tag{23}$$

Inner boundary condition is as follows.

$$C\frac{dp_w}{dt} - \left[\frac{2\pi rhk_{fi}e^{\gamma(p_f - p_i)}}{\mu}\left(\frac{\partial p}{\partial r}\right)\right]_{r=r_w} = -qB, \tag{24}$$

$$p_w = \left(p_f - Sr_w\frac{\partial p_f}{\partial r}\right)\Big|_{r=r_w} \tag{25}$$

Considering the outer boundary as the elastic boundary, outer boundary condition can be obtained as follows.

$$\left[\varepsilon_\Gamma^{P_f} p_f + r\frac{\partial p_f}{\partial r}\right]\Big|_{r=R} = 0$$

Dimensionless mathematical model

For convenience, the following dimensionless variables are defined.

Dimensionless pressure $p_D = \dfrac{2\pi k_{fi} h}{qB\mu}\Delta p \quad (\Delta p = p_i - p)$

Storage ratio $\omega = \dfrac{\phi_{fi} C_{ft}}{\phi_{fi} C_{ft} + \phi_{m0} C_{mt}}$

Dimensionless interporosity flow coefficient $\lambda = \alpha (k_m / k_{fi}) r_w^2$

Dimensionless time $t_D = \dfrac{k_{fi} t}{(\phi_{fi} C_{ft} + \phi_{mi} C_{mt})\mu r_w^2}$

Dimensionless wellbore storage $C_D = \dfrac{C}{2\pi(\phi_{mi} c_{ft} + \phi_{fi} c_{mt}) h r_w^2}$

Dimensionless permeability modulus $\gamma_D = \dfrac{qB\mu}{2\pi k_{fi} h}\gamma$

Introducing these dimensionless variables, the following equations can be obtained from Eqs. 19 and 21~26.

$$(1-\omega)\frac{\partial p_{mD}}{\partial t_D} + \lambda(p_{mD} - p_{fD}) = 0 \tag{27}$$

$$\frac{\partial^2 p_{fD}}{\partial r_D^2} + \frac{1}{r_D}\frac{\partial p_{fD}}{\partial r_D} - \gamma_D\left[\frac{\partial p_{fD}}{\partial r_D}\right]^2 = e^{\gamma_D p_{fD}}\left[\omega\frac{\partial p_{fD}}{\partial t_D} + \lambda(p_{fD} - p_{mD})\right] \tag{28}$$

$$p_{fD}(r_D, t_D)\big|_{t_{D=0}} = 0 \tag{29}$$

$$p_{mD}(r_D, t_D)\big|_{t_{D=0}} = 0 \tag{30}$$

$$C_D\frac{dp_{wD}}{dt_D} - \left(r_D e^{\alpha(p_f - p_i)}\frac{\partial p_{fD}}{\partial r_D}\right)\Bigg|_{r_D=1} = 1 \tag{31}$$

$$p_{wD} = \left(p_{fD} - S\frac{\partial p_{fD}}{\partial r_D}\right)\Bigg|_{r_D=1} \tag{32}$$

$$\left[\varepsilon_\Gamma^{P_{fD}} p_{fD} + r_D\frac{\partial p_{fD}}{\partial r_D}\right]\Bigg|_{r_D=R_D} = 0 \tag{33}$$

The dimensionless well radius is introduced as follows:

$$r_{De} = r_D e^S \tag{34}$$

Taking $T_D = t_D / C_D$,

$$\frac{\partial^2 p_{fD}}{\partial r_{De}^2} + \frac{1}{r_{De}}\frac{\partial p_{fD}}{\partial r_{De}} - \gamma_D\left[\frac{\partial p_{fD}}{\partial r_D}\right]^2 = e^{\gamma_D p_{fD}}\left[\frac{\omega}{C_D e^{2S}}\frac{\partial p_{fD}}{\partial T_D} + \lambda e^{-2S}(p_{fD} - p_{mD})\right], \tag{35}$$

$$\frac{(1-\omega)}{C_D e^{2S}}\frac{\partial p_{mD}}{\partial T_D} + \lambda e^{-2S}(p_{mD} - p_{fD}) = 0, \tag{36}$$

$$\frac{dp_{wD}}{dT_D} - \left(r_{De} e^{\gamma_D p_{fD}}\frac{\partial p_{fD}}{\partial r_{De}}\right)\Bigg|_{r_{De}=1} = 1, \tag{37}$$

$$p_{wD} = p_{fD}(1, T_D), \tag{38}$$

$$p_{fD}(r_D, T_D)\big|_{t_{D=0}} = 0, \tag{39}$$

$$p_{mD}(r_D, T_D)\big|_{T_{D=0}} = 0, \tag{40}$$

$$\left[\varepsilon_\Gamma^{P_{fD}} p_{fD} + r_{De}\frac{\partial p_{fD}}{\partial r_{De}}\right]\Bigg|_{r_{De}=R_{De}} = 0, \tag{41}$$

where $R_{De} = R_D e^S$.

Solution of model

The seepage differential equation, Eq. 35 for fracture system and inner boundary condition, Eq. 37 have strong nonlinearity. Therefore, to linearize these equations, Pedrosa 's transformation and perturbation transformation are applied

Pedrosa 's transformation is as follows (Pedrosa, 1986):

$$p_{fD}(r_D, T_D) = -\frac{1}{\gamma_D}\ln[1 - \gamma_D \xi_{fD}] \tag{42}$$

Applying Pedrosa 's transformation, Eq. 42, and rearranging it,

$$\frac{\partial^2 \xi_{fD}}{\partial r_{De}^2} + \frac{1}{r_{De}}\frac{\partial \xi_{fD}}{\partial r_{De}} = \frac{\omega}{C_D e^{2S}}\frac{\partial p_{fD}}{\partial T_D} + \lambda e^{-2S}(p_{fD} - p_{mD}), \tag{43}$$

$$\frac{d\xi_{wD}}{dT_D} - \left(r_{De}\frac{\partial \xi_{fD}}{\partial r_{De}}\right)\Bigg|_{r_{De}=1} = 1, \tag{44}$$

$$\xi_{wD} = \xi_{fD}(1, T_D), \tag{45}$$

$$\xi_{fD}(r_D, T_D)\big|_{T_{D=0}} = 0, \tag{46}$$

$$p_{mD}(r_D, T_D)\big|_{T_{D=0}} = 0, \tag{47}$$

$$\left\{-\frac{\varepsilon_\Gamma^{P_{fD}}}{\gamma_D}\ln[1-\gamma_D\xi_{fD}] + \frac{1}{1-\gamma_D\xi_{fD}} r_{De}\frac{\partial \xi_{fD}}{\partial r_{De}}\right\}\Bigg|_{r_{De}=R_{De}} = 0. \tag{48}$$

Perturbation transformation

The perturbation transformation is as follows (Pedrosa, 1986):

$$\xi_{fD} = \xi_{fD0} + \gamma_D\xi_{fD1} + \gamma_D^2\xi_{fD2} + \cdots \approx \xi_{fD0}, \tag{49}$$

$$-\frac{1}{\gamma_D}\ln[1-\gamma_D\xi_{fD}] = \xi_{fD} + \frac{1}{2}\gamma_D\xi_{fD}^2 + \cdots \approx \xi_{fD}, \tag{50}$$

$$\frac{1}{1-\gamma_D\xi_{fD}} = 1 + \gamma_D\xi_{fD} + \gamma_D^2\xi_{fD}^2 + \cdots \approx 1. \tag{51}$$

As the value of γ_D is small, the solution of zero-order perturbation can satisfy the accuracy requirement.

$$\frac{\partial^2 \xi_{fD0}}{\partial r_{De}^2} + \frac{1}{r_{De}}\frac{\partial \xi_{fD0}}{\partial r_{De}} = \frac{\omega}{C_D e^{2S}}\frac{\partial p_{fD}}{\partial T_D} + \lambda e^{-2S}(p_{fD} - p_{mD}) \tag{52}$$

$$\frac{d\xi_{wD0}}{dT_D}-\left(r_{De}\frac{\partial\xi_{fD0}}{\partial r_{De}}\right)\Bigg|_{r_{De}=1}=1 \tag{53}$$

$$\xi_{wD0}=\xi_{fD0}(1,T_D) \tag{54}$$

$$\xi_{fD0}(r_D,T_D)\big|_{T_{D=0}}=0 \tag{55}$$

$$p_{mD}(r_D,T_D)\big|_{T_{D=0}}=0 \tag{56}$$

$$\left[\varepsilon_\Gamma^{P_{fD}}\xi_{fD0}+r_{De}\frac{\partial\xi_{fD0}}{\partial r_{De}}\right]\Bigg|_{r_{De}=R_{De}}=0 \tag{57}$$

Laplace transformation

The Laplace transformation of Eqs. 36 and 52~57 is taken with respect to T_D.

The Laplace transformation is defined as follows:

$$\bar{\xi}_{fD0}(r_{De},z)=\int_0^\infty e^{-zT_D}\xi_{fD0}(r_{De},T_D)dT_D\,, \tag{58}$$

$$\bar{p}_{fD}(r_{De},z)=\int_0^\infty e^{-zT_D}p_{fD}(r_{De},T_D)dT_D\,, \tag{59}$$

$$\bar{p}_{mD}(r_{De},z)=\int_0^\infty e^{-zT_D}p_{mD}(r_{De},T_D)dT_D\,, \tag{60}$$

$$\frac{\partial^2\bar{\xi}_{fD0}}{\partial r_{De}^2}+\frac{1}{r_{De}}\frac{\partial\bar{\xi}_{fD0}}{\partial r_{De}}=\frac{\omega}{C_De^{2S}}z\bar{p}_{fD}+\lambda e^{-2S}(\bar{p}_{fD}-\bar{p}_{mD}) \tag{61}$$

$$\frac{(1-\omega)}{C_De^{2S}}z\bar{p}_{mD}+\lambda e^{-2S}(\bar{p}_{mD}-\bar{p}_{fD})=0 \tag{62}$$

$$z\bar{\xi}_{wD0}-\left(r_{De}\frac{\partial\bar{\xi}_{fD0}}{\partial r_{De}}\right)\Bigg|_{r_{De}=1}=\frac{1}{z} \tag{63}$$

$$\bar{\xi}_{wD0}=\bar{\xi}_{fD0}(1,T_D) \tag{64}$$

$$\left[\varepsilon_\Gamma^{P_{fD}}\bar{\xi}_{fD0}+r_{De}\frac{\partial\bar{\xi}_{fD0}}{\partial r_{De}}\right]\Bigg|_{r_{De}=R_{De}}=0 \tag{65}$$

Substituting Eq. 62 into Eq. 61 and rearranging,

$$\frac{\partial^2\bar{\xi}_{fD0}}{\partial r_{De}^2}+\frac{1}{r_{De}}\frac{\partial\bar{\xi}_{fD0}}{\partial r_{De}}-f(z)\cdot\bar{\xi}_{fD0}=0\,, \tag{66}$$

where $$f(z)=\frac{z}{c_De^{2s}}\left[\frac{\omega(1-\omega)\dfrac{z}{c_De^{2s}}+\lambda e^{-2s}}{(1-\omega)\dfrac{z}{c_De^{2s}}+\lambda e^{-2s}}\right]. \tag{67}$$

The general solution of Eq. 66 is as follows:

$$\bar{\xi}_{fD0}(r_{De},z)=AK_0\left(r_{De}\sqrt{f(z)}\right)+BI_0\left(r_{De}\sqrt{f(z)}\right), \tag{68}$$

$$\frac{\partial\xi_{fD0}}{\partial r_{De}}=-A\sqrt{f(z)}K_1\left(r_{De}\sqrt{f(z)}\right)+B\sqrt{f(z)}I_1\left(r_{De}\sqrt{f(z)}\right). \tag{69}$$

Substituting Eqs. 68 and 69 into Eqs. 63 and 65, and rearranging,

$$A\left[zK_0\left(\sqrt{f(z)}\right)+\sqrt{f(z)}K_1\left(\sqrt{f(z)}\right)\right]+B\left[I_0\left(\sqrt{f(z)}\right)-\sqrt{f(z)}I_1\left(\sqrt{f(z)}\right)\right]=\frac{1}{z}, \tag{70}$$

$$A\left[-\varepsilon_\Gamma^{P_{fD}}K_0\left(R_{De}\sqrt{f(z)}\right)+R_{De}\sqrt{f(z)}K_1\left(R_{De}\sqrt{f(z)}\right)\right]-B\left[R_{De}I_1\left(R_{De}\sqrt{f(z)}\right)-\varepsilon_\Gamma^{P_{fD}}I_0\left(R_{De}\sqrt{f(z)}\right)\right]=0 \tag{71}$$

Solving Eqs. 70 and 71 simultaneously, A and B can be obtained as follows:

$$A=a_4/\left[z(-a_3a_2+a_1a_4)\right], \tag{72}$$

$$B=-a_3/\left[z(-a_3a_2+a_1a_4)\right], \tag{73}$$

where $a_1=zK_0\left(\sqrt{f(z)}\right)+\sqrt{f(z)}K_1\left(\sqrt{f(z)}\right)$,

$a_2=zI_0\left(\sqrt{f(z)}\right)-\sqrt{f(z)}I_1\left(\sqrt{f(z)}\right)$,

$a_3=-\varepsilon_\Gamma^{P_{fD}}K_0\left(R_{De}\sqrt{f(z)}\right)+R_{De}\sqrt{f(z)}K_1\left(R_{De}\sqrt{f(z)}\right)$

$a_4=-\varepsilon_\Gamma^{P_{fD}}I_0\left(R_{De}\sqrt{f(z)}\right)-R_{De}\sqrt{f(z)}I_1\left(R_{De}\sqrt{f(z)}\right)$.

From Eq. 64,

$$\bar{\xi}_{wD0}=\bar{\xi}_{fD0}(1,T_D)=AK_0\left(\sqrt{f(z)}\right)+BI_0\left(\sqrt{f(z)}\right). \tag{74}$$

When $x\to\infty$, the values of 0th and 1st order Bessel functions of the first kind converge to infinity. Therefore, these values cannot be calculated by using computer. In order to avoid this, the following asymptotic formula is used.

$$I_\gamma(x)=\frac{e^x}{\sqrt{2\pi x}}\left[1+0\left(\frac{1}{x}\right)\right]\approx\frac{e^x}{\sqrt{2\pi x}} \tag{75}$$

Substituting Eq. 75 into Eq. 74 and rearranging,

$$\bar{\xi}_{wD0}=AK_0\left(\sqrt{f(z)}\right)+BI_0\left(\sqrt{f(z)}\right)$$

$$=\frac{\frac{e^{R_{De}f(z)}}{\sqrt{2\pi R_{De}f(z)}}\left[\varepsilon_\Gamma^{P_{fD}}+R_{De}\sqrt{f(z)}\right]K_0\left(\sqrt{f(z)}\right)-\left[\varepsilon_\Gamma^{P_{fD}}K_0\left(R_{De}\sqrt{f(z)}\right)-R_{De}\sqrt{f(z)}K_1\left(R_{De}\sqrt{f(z)}\right)\right]\frac{e^{f(z)}}{\sqrt{2\pi f(z)}}}{\frac{e^{R_{De}f(z)}}{\sqrt{2\pi R_{De}f(z)}}\left[zK_0\left(\sqrt{f(z)}\right)+\sqrt{f(z)}K_1\left(\sqrt{f(z)}\right)\right]\left[\varepsilon_\Gamma^{P_{fD}}+R_{De}\sqrt{f(z)}\right]}\cdot \tag{76}$$

When $R_{De}f(z)\to\infty$, from Eq. 76, the following equation is obtained.

$$\bar{\xi}_{wD0}=\frac{K_0\left(\sqrt{f(z)}\right)}{zK_0(f(z))+f(z)K_1(f(z))}. \tag{77}$$

ξ_{wD0} is obtained by numerically inverting Laplace transformation, Eqs. 76 and 77. In order to numerically invert Laplace transformation, the algorithm by Kim et al. (2021b) is used, where n=25, a=6.5, k=2, σ=0.

Pressure is calculated with Eq. 42 and pressure derivative with the following equation.

$$T_D \frac{\partial p_{fD}}{\partial T_D} = -T_D \frac{\partial \xi_{fD}}{\partial T_D} \Big/ \left(\gamma_D \xi_{fD} - 1\right)$$

Result and Discussion

Verification of model

Comparison verification

To verify our model, this is compared to the model for the DPR with EOB without consideration of the stress sensitivity. When stress sensitivity is not considered in this model, as there is permeability modulus in denominator of Eq. 42 and it converges into infinity, (here). Other parameters are as follows: RDe=2000,. Figure.2 shows the result of comparison of two models. The solid lines represent our model and circle mark the dual-porosity without consideration of stress sensitivity (Kim et al., 2021a). From Figure.2, it can be seen that two models agree well, which shows that our model is valid.

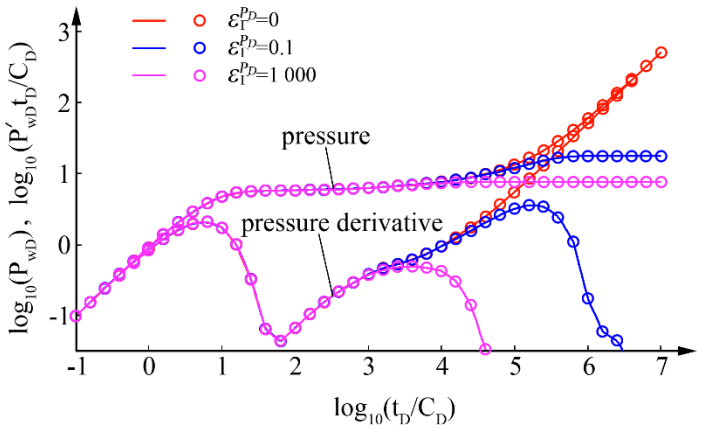

Figure 2: Result of comparison of our model to the model without consideration of stress sensitivity

Analysis of Sensitivity

Effect of permeability modulus on the PPD curves

Figure.3 shows the effect of the permeability modulus (=0.001, 0.1, 0.2, 0.3) on the PPD curves. Other parameters are as follows: CDe2S=100, , λ=10-3, ω=10-5, RDe=2 000. As shown in Figure.3, the larger value of, the higher PPD curves. As time increase, the effect of the permeability modulus on PPD curves increases. When, horizontal line of value 0.5 does not appear in the middle stage of pressure derivative curve. This means that the SSP affects analysis of the well-testing data.

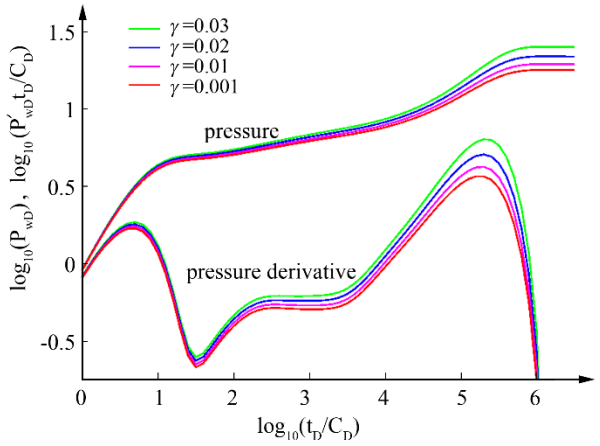

Figure 3. Effect of gamma on the PPD curves

Effect of elastic coefficient of outer boundary on the PPD curves

According to Li et al. (2019a), reflects the closed boundary, the constant pressure boundary, the infinite boundary and between closed boundary and constant pressure boundary.

Figure.4 shows the effect of elastic coefficient (=0, 0.1, 1, 1000) of outer boundary on the PPD curves. Other parameters are as follows: CDe2S=100, λ=10-3, ω=10-5, RDe=2 000. As shown in Figure.5, does not affect the early and middle stages of the pressure derivative curves, but affects the late stage of the pressure derivative curves. When the value of is zero, it reflects the closed boundary. While, when the value of is 1 000, it reflects that is close to the closed boundary. Moreover, when, it reflects the infinite boundary. This means that with the value of, the middle stage of PPD curves are between closed boundary and constant pressure boundary. However, the outer boundary condition between closed boundary and constant pressure boundary has not been considered at the model of reservoir with the ideal outer boundary (infinite boundary, closed boundary and constant pressure boundary). Thus, our model has generality in comparison to the model with ideal outer boundary. Therefore, this means that the accuracy of well-testing analysis can be enhanced.

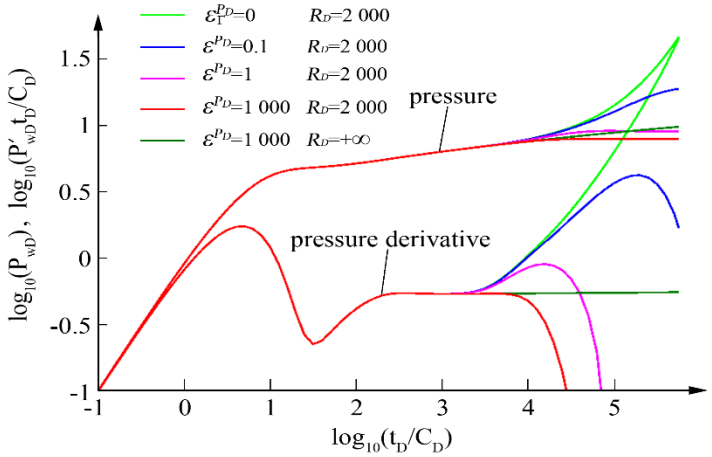

Figure.4. Effect of elastic coefficient of outer boundary on the PPD curves

Effect of CDe2S on the PPD curves

CDe2S is a dimensionless quantity, which considers wellbore storage and skin simultaneously, and shows degrees of improvement or damage of well.

Figure.5 shows the effect of CDe2S (CDe2S=1000, 2 000, 5 000, 10 000) on the PPD curves. Other parameters are as follows:, =0.01, , λ=10-5, ω=10-5, RDe=2 000. CDe2S affects the middle stage of pressure curve. The lager the value of CDe2S increases, the upper the pressure derivative curves are in the middle stage and the earlier the effect of boundary appears on the pressure derivative curves.

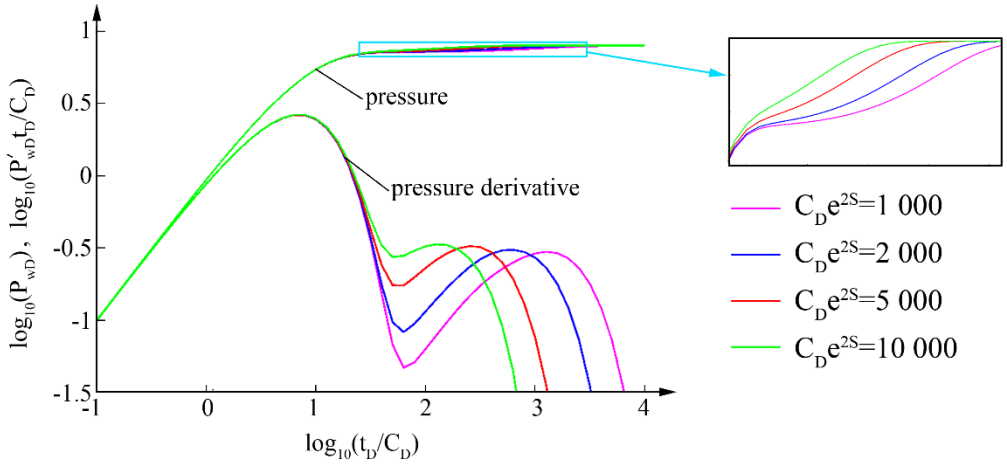

Figure 5: Effect of C_De^{2S} on the PPD curves

Effect of skin S on the PPD curves

Figure.6 shows the effect of skin S (S=-3, -1, 0, 1, 3) on the PPD curves. Other parameters are as follows: =0.01, λ=10-3, ω=10-4, CDe2S=10, RD=5 000. Skin S affects the middle and late stages of the PPD. The smaller value of S decreases, the upper the PPD curves are, the higher "hump" of the pressure derivative curve gets, and the later it appears.

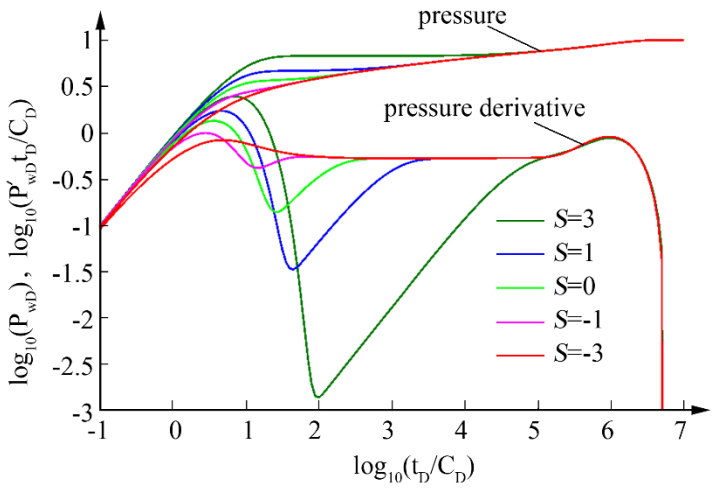

Figure 6: Effect of skin S on the PPD curves

Effect of dimensionless radius RD on the PPD curves

Figure.7 shows effect of dimensionless radius RD (RD =100, 1 000, 5 000, 10 000) on the PPD curves. Other parameters are as follows: =0.01, , λ=10–3, ω=10-5, CDe2S=1 000,. RD affects only the late stage of the PPD curves. The larger the value of RD increases, the later the effect of boundary appears.

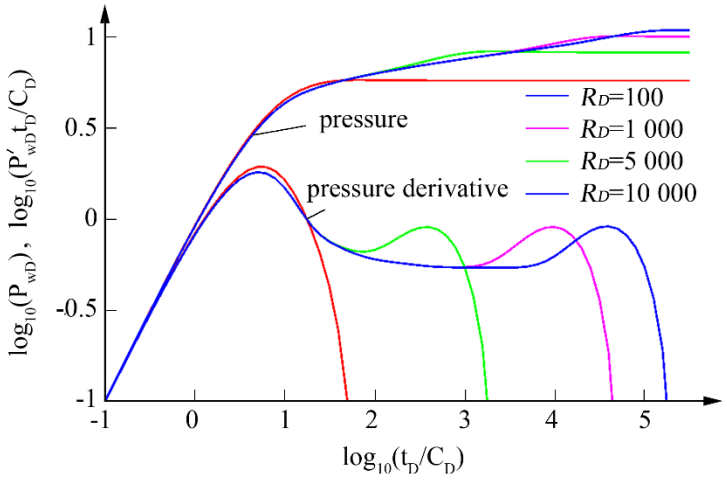

Figure 7: Effect of dimensionless radius RD on the PPD curves

Effect of inter-porosity flow coefficient on the PPD curves

Figure.8 shows effect of inter-porosity flow coefficient (=10-2, 10-3, 10-4) on the PPD curves. Other parameters are as follows: =0.01, ω=10-4, CDe2S=10, RD=5 000. The inter-porosity flow coefficient affects the middle stage of the PPD curves. The larger the value of increases, the upper the PPD curves are, the higher "hump" of the pressure derivative curve gets, the deeper the concave of the pressure derivative curve are and the later the concave appears.

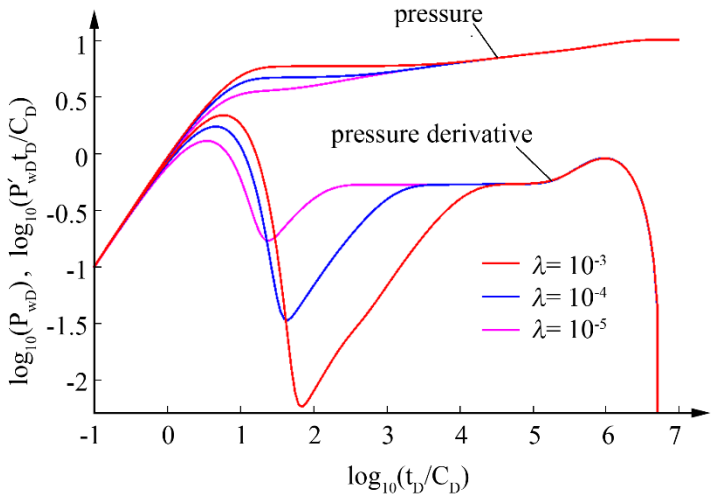

Figure 8: Effect of inter-porosity flow coefficient λ on the PPD curves

Effect of storage ratio on the PPD curves

Figure.9 shows effect of storage ratio (=10-1, 10-2, 10-3, 10-4) on the PPD curves. Other parameters are as follows: =0.01, =10-4, CDe2S=10, , RD=5 000. affects both the early and middle period of flow. The smaller the upper the pressure curves are, the higher "hump" of the pressure derivative curve gets, the deeper the concave are and the earlier the concave appears.

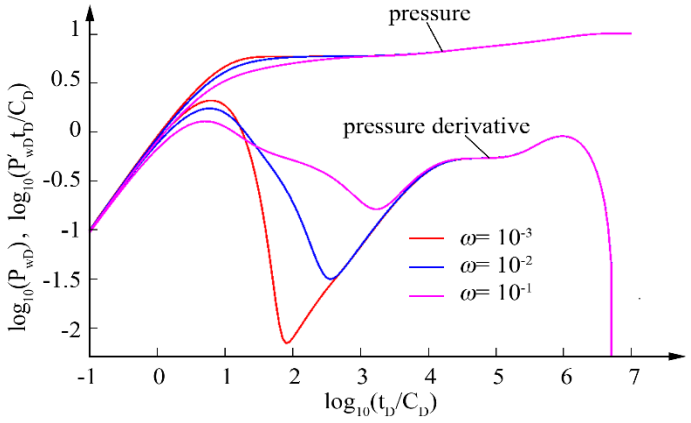

Figure 9: Effect of storage ratio ω on the PPD curves

Both the SSP and the condition of elasticity of the outer boundary greatly affect the well-testing analysis, but the previous papers have considered these effects individually and have not considered simultaneously, which may result in the considerable errors in the well-testing analysis. The well-testing model proposed in our paper considers the effect of the SSP and the condition of elasticity of the outer boundary simultaneously. Thus, this model may improve the accuracy of the well-testing analysis for the DPR.

There are also several models including the triple-porosity model. However, this model is limited to the dual-porosity model for vertical well. We are going to study the triple-porosity dual-permeability model for horizontal and inclined well considering EOB.

Conclusion

Based on the consideration of stress sensitivity and elastic outer boundary conditions, we first formulated the seepage differential equation in the dual-porosity reservoir considering wellbore storage and skin factor, and defined the dimensionless variable to facilitate the derivation of the solution.

This mathematical model is strong nonlinear, the Pedrosa' s transformation is applied.

However, after the transformation of Pedrosa is applied, the mathematical model is still nonlinear, So the perturbation transformation is performed to eliminate the nonlinearity of the model, and then the Laplace transformation is performed to obtain the analytical solution of the well test model in the dual-porosity reservoir considering elastic outer boundary and stress sensitivity in the Laplace space, and the Laplace numerical inversion (Kim etc., 2021b) is applied to obtain the dimensionless pressure and pressure derivative model curve in the wellbore.

To verify the accuracy of the model, we verified that the model is valid compared with the dual-porosity reservoir model (Kim etc., 2021a) with the elastic boundary without considering stress sensitivity, we performed a parametric sensitivity analysis on the pressure and pressure derivative curve and showed that the elastic outer boundary and stress sensitivity affect the well- test data analysis.

The model presented in this paper can improve the accuracy of well-test data analysis compared to the well test model in the previous dual-porosity reservoir.

Nomenclature

B-Volume factor, dimensionless

C- wellbore storage coefficient, m3/Pa

CD-Dimensionless wellbore storage, dimensionless

Cm, Cf-Compressibility of matrix system and natural fracture system, respectively, Pa-1

Cmt-Total compressibility of matrix system and oil, Pa-1

Cft-Total compressibility of natural fracture system and oil, Pa-1

Co-Oil compressibility, Pa-1

km, kf-Permeability of matrix system and natural fracture system, respectively, m2

kfi-Permeability of natural fracture under initial condition, m2

h- Reservoir thickness, m

p-Reservoir pressure, Pa

R- outer boundary radius, m

RD- dimensionless outer boundary radius, dimensionless

pm, pf-Pressure in matrix system and natural fracture system, respectively, Pa

pi-Initial reservoir pressure, Pa

pw-Wellbore pressure, Pa

q-Well rate, m3/s

q*-Mass flow velocity between matrix system and fracture system in the reservoir of unit volume, kg/(m3s)

r-Radius, m rw-Well radius, m

S- skin, dimensionless

t-Time, s

tD-Dimensionless time, dimensionless

z-Laplace variable, dimensionless

-Shape factor between matrix and fracture, m-2

-Oil density at pressure pm in the matrix system and at pressure pf in natural fracture system, respectively, kg/m3

-Oil density under initial condition, kg/m3

- Permeability modulus, Pa-1

-Dimensionless permeability modulus, dimensionless

-Dimensionless inter-porosity flow coefficient, dimensionless

- Storage ratio, dimensionless

-Viscosity of oil, Pa·s.

-Porosity of matrix system and natural fracture system, respectively, fraction

-Porosity of matrix system and natural fracture system under initial condition, respectively, fraction

-Flow velocity of fluid in matrix system and natural fracture system, respectively, m/s

Superscripts

- Laplace transformation

Subscripts

D-Dimensionless

m-Matrix

f-Fracture

w-Well

Acknowledgement

We gratefully acknowledge all professors of Petroleum Institute, Faculty of Geoscience and Technology, Kim Chaek University of Technology for her valuable suggestions and discussions.

Reference

1. Aguilera, R., (2008). Effect of fracture compressibility on gas-in-place calculation of stress-sensitive naturally fractures reservoirs. April 2008 SPE Reservoir Evaluation & Engineering, 307-310.
2. Chilingar, George V., Rieke, H. H., Al-Anazi, Ammal F., (2005). Why many overpressured, stress-sensitive hydrocarbon reservoirs should not be abandoned. Energy Sources, Part A: Recovery, Utilization, and Environmental Effects, 27(16), 1495-1501.
3. Du, D., Zhang, G., Zhao, Y., Sun, X., Zhang, B., (2020). Transient flow theory of multiple-fractured horizontal wells with complex mechanisms in shale gas reservoirs. Geofluids Volume 2020, Article ID 7364734, 17 pages.
4. Cao, C., Cheng, L., Zhang, X., Shi, J, (2021). Numerical simulation investigation on well performance integrated stress sensitivity and sand production. Geofluids Volume 2021, Article ID 9925866, 11 pages.
5. Chen, Z., Liao, X., Zhao, X., Dou, X., Zhu, L., (2016). A semi-analytical mathematical model for transient pressure behavior of multiple fractured vertical well in coal reservoirs incorporating with diffusion, adsorption and stress-sensitivity. Journal of Natural Gas Science and Engineering 29, 570-582.
6. Chen, J., Song, X., Li, B., Li, W., Liao, C., Yang, L., (2021). Mathematical simulation about gas transport in a dual-porosity tight gas reservoir considering multiple effects. Geofluids Volume 2021, Article ID 7483445, 7 pages.
7. Feng, Y., Liu, Y., Lei, G., (2021). Study on stress-dependent permeability of fracture networks in fractured porous media. Geofluids Volume 2021, Article ID 7433547, 19 pages.
8. Gamal, Rezk, M., (2016). Analysis of Pressure Transient Tests in Naturally Fractured Reservoirs. Oil Gas Res 2: 121.
9. Gao, Y., Jiang, R., Xu, X., Sun, Z., Yuan, Z., Ma, K., Jiang, B., Kang, B., Chen, G., Li, C., (2021). The Pressure Buildup Well Test Analysis considering Stress Sensitivity Effect for Deepwater Composite Gas Reservoir with High Temperature and Pressure. Geofluids Volume 2021, Article ID 5054246, 16 pages.
10. Guo, C., Xu, J., Wei, M., Jiang, R., (2015). Pressure transient and rate decline analysis for hydraulic fractured vertical wells with finite conductivity in shale gas reservoirs. J Petrol Explor Prod Technol 5, 435-443.
11. Guo, J., Meng, F., Jia, A., Dong, S., Yan, H., Zhang, H., Tong, G., (2021). Production behavior evaluation on multilayer commingled stress-sensitive carbonate gas reservoir. Energy Exploration & Exploitation 39(1), 86-107.
12. Huang, Y., Li, X., Tan, X., (2018) a. Transient pressure and rate decline analysis for horizontal well in stress-sensitive composite reservoir. Mathematical Problems in Engineering Volume 2018, Article ID 8672578
13. Huang, S., Yao, Y., Zhang, S., Ji, J., Ma, R., (2018). b. Pressure transient analysis of multi-fracture horizontal wells in tight oil reservoirs with consideration of stress sensitivity. Arabian Journal of Geosciences volume 11, Article number. 285
14. Jabbari, H., Zeng, Z., Korom, S. F., Khavanin, M., (2012). Well test analysis in dual-porosity aquifers with stress-dependent conductivity. Research Journal of Environmental and Earth Sciences 4(11), 962-981.

15. Jelmert, T. A., Toverud, T., (2017). Compaction in a confined deforming reservoir. Energy Procedia 128, 165–171.
16. Ji, J., Yao, Y., Huang, S., Ma, X., Zhang, S., Zhang, F., (2017). Analytical model for production performance analysis of multi-fractured horizontal well in tight oil reservoirs. Journal of Petroleum Science and Engineering 158, 380-397.
17. Jiang, J., Yang, J., (2018). Coupled fluid flow and geomechanics modeling of stress-sensitive production behavior in fractured shale gas reservoirs. International Journal of Rock Mechanics and Mining Sciences 101, 1-12.
18. Kim, S. C., Han, C. G., Rim, M. W., Kim, J. S., Ryang. M. J., (2021) a, Analyzing fluid flow characteristics in a dual-porosity reservoir with an elastic outer boundary. Acta Geophysica 69, 1843-1853.
19. Kim, S.C., Song, Y.I., Han, C.G., (2021) b. Improved numerical inverse Laplace transformation to improve the accuracy of type curve for analyzing well-testing data. Acta Geophysica 69, 919-930.
20. Li, X.-P., Cao, L.-N., Luo, C., Zhang, B., Zhang, J.-Q., Tan, X.-H., (2017). Characteristics of transient production rate performance of horizontal well in fractured tight gas reservoirs with stress-sensitivity effect. Journal of Petroleum Science and Engineering 158, 92–106..
21. Li, S., Zhao, C., Zheng, P., Gui, Q., (2019) a. Analysis of oil and gas flow characteristics in the reservoir with the elastic outer boundary. Journal of Petroleum Science and Engineering 175, 280-285.
22. Li, Z., Wu, X., Han, G., Ma, G., Zhang, L., Wang, B., Shi, S., (2019) b. Transient pressure analysis of volume-fractured horizontal wells considering complex fracture networks and stress sensitivity in tight reservoirs. ACS Omega 4(11), 14466–14477.
23. Li, Z., Qi, Z., Yan, W., Xiang, Z., Ao, X., Huang, X., Mo, F., (2020) a. Prediction of production performance of refractured shale gas well considering coupled multiscale gas flow and geomechanics. Geofluids Volume 2020, Article ID 9160346, 21 pages.
24. Li, S., Guo, H., Zheng, P., Dong, X., Zhao, C., Gui, Q., (2020) b. The elastic boundary value problem of extended modified Bessel equation and its application in fractal homogeneous reservoir. Computational and Applied Mathematics (2020) 39:63, 1-16.
25. Liu, M., Xiao, C., Wang, Y., Li, Z., Zhang, Y., Chen, S., Wang, G., (2015). Sensitivity analysis of geometry for multi-stage fractured horizontal wells with consideration of finite-conductivity fractures in shale gas reservoirs. Journal of Natural Gas Science and Engineering 22, 182-195.
26. Liu, H., (2017). The numerical simulation for multistage fractured horizontal well in low-permeability reservoirs based on modified Darcy's equation. J Petrol Explor Prod Technol 7, 735-746.
27. Luo, A., Li, Y., Wu, L., Peng, Y., Tang, W., (2021). Fractured horizontal well productivity model for shale gas considering stress sensitivity, hydraulic fracture azimuth, and interference between fractures. Natural Gas Industry B 8, 278-286.
28. Meng, F., Lei, Q., He, D., Yan, H., Jia, A., Deng, H., Xu, W., (2018). Production performance analysis for deviated wells in composite carbonate gas reservoirs. Journal of Natural Gas Science and Engineering 56, 333–343.
29. Mo, S., He, S., Lei, G., Gai, S., (2016). Deliverability equation in pseudo-steady state for fractured vertical well in tight gas. J Petrol Explor Prod Technol 6, 33-38.
30. Moradi, M., Shamloo, A., Asadbegi, M., Dezfuli, A.D., (2017). Three dimensional pressure transient behavior study in stress sensitive reservoirs. Journal of Petroleum Science and Engineering 152 (2017), 204–211.
31. Pedrosa, O. A., (1986). Pressure transient response in stress-sensitive formations. SPE 15115.
32. Samaniego, V. F., Villalobos, L. H., (2003). Transient pressure analysis of pressure-dependent naturally fractured reservoirs. Journal of Petroleum Science and Engineering 39, 45-56.
33. Ren, J., Guo, P., (2018). A general analytical method for transient flow rate with the stress-sensitive effect. Journal of Hydrology (2018)
34. Selvadurai, A.P.S., Zhang, D., Kang, Y., 2018. Permeability evolution in natural fractures and their potential influence on loss of productivity in ultra-deep gas reservoirs of the Tarim Basin, China. Journal of Natural Gas Science and Engineering 58, 162-177.
35. Shi, J., Wang, S., Wang, K., Liu, C., Wu, S., Sepehrnoori, K., (2019). An accurate method for permeability evaluation of undersaturated coalbed methane reservoirs using early dewatering data. International Journal of Coal Geology 202, 147–160.
36. Shovkun, I., Espinoza, D. N., (2017). Coupled fluid flow-geomechanics simulation in stress-sensitive coal and shale reservoirs: Impact of desorption-induced stresses, shear failure, and fines migration. Fuel 195, 260-272.
37. Shu, Y., Yan, J., (2008). Characterization and prevention of formation damage for fractured carbonate reservoir formations with low permeability. Pet. Sci 5, 326-333.
38. Tian, X., Cheng, L., Zhao, W., Yan, Y., He, X., Guo, Q., (2015). Experimental study on permeability stress sensitivity in tight sandstone oil reservoirs. Sains Malaysiana 44(5), 719-725
39. Tian, L., Zhang, K., Liu, G., Guo, J., (2017). A Well testing model on pressure characteristics of the heterogeneous composite gas reservoir. GeoConvention (2017), 1-10.
40. Wang, R., Yue, X., Zhao, R., Yan, P., Dave, F., (2009). Effect of stress sensitivity on displacement efficiency in CO2 flooding for fractured low permeability reservoirs. Pet. Sci. 6, 277-283.
41. Wang, Z., Ran, B., Tong, M., Wang, C., Yue, Q., (2014). Forecast of fractured horizontal well productivity in dual permeability layers in volcanic gas reservoirs. PETROLEUM EXPLORATION AND DEVELOPMENT 41(5), 642-647.
42. Wang, L., Wang, X., (2016). Modelling of pressure transient behaviour for fractured gas wells under stress-sensitive and slippage effects. Int. J. Oil, Gas and Coal Technology 11(1), 18-38.
43. Wang, H., Guo, J., Zhang, L., (2017) a. A Semi-analytical model for multilateral horizontal wells in low-permeability naturally fractured reservoirs. Journal of Petroleum Science and Engineering 149, 564-578.
44. Wang, H., Ran, Q., Liao, X., (2017) b. Pressure transient responses study on the hydraulic volume fracturing vertical well in stress sensitive tight hydrocarbon reservoirs. International Journal of Hydrogen Energy 42, 18343-18349.
45. Wang, J., Jia, A., Wei, Y., Qi, Y., (2017)c. Approximate semi-analytical modeling of transient behavior of horizontal well intercepted by multiple pressure-dependent conductivity fractures in pressure sensitive reservoir. Journal of Petroleum Science and Engineering 153, 157-177.
46. Wang, L., Yang, S., Meng, Z., Chen, Y., Qian, K., Han, W., Wang, D., (2018). Time dependent shape factors for fractured reservoir simulation: Effect of stress sensitivity in matrix system. Journal of Petroleum Science and Engineering 163, 556-569.
47. Wang, G., Jia, A., Wei, Y., Xiao, C., (2020). Transient pressure analysis for multifractured horizontal well with the use of multilinear flow model in shale gas reservoir. Geofluids Volume 2020, Article ID 8348205, 20 pages.
48. Wang, H., Kou, Z., Guo, J., Chen, Z., (2021). A semi-analytical model for the transient pressure behaviors of a multiple fractured well in a coal seam gas reservoir. Journal of Petroleum Science and Engineering 198, March 2021, 108159

49. Warren, J.E., Root, P.J., (1963). The behavior of naturally fractured reservoirs. SPE Journal. 3(3), 245-255..
50. Wu, Z., Cui, C., Wang, Z., Sui, Y., Jia, P., Tang, W., (2018)a. Well testing model of multiple fractured horizontal well with consideration of stress-sensitivity and variable conductivity in tight gas reservoirs. Mathematical Problems in Engineering Volume 2018, Article ID 1693184, 13 pages.
51. Wu, Z., Cui, C., Lv, G.., Bing, S., Cao, G.., (2018)b. A multi-linear transient pressure model for multistage fractured horizontal well in tight oil reservoirs with considering threshold pressure gradient and stress sensitivity. Journal of Petroleum Science and Engineering 172, 839-854..
52. Wu, M., Ding, M., Yao, J., Xu, S., Li, L., Li, X., (2018) c. Pressure transient analysis of multiple fractured horizontal well in composite shale gas reservoirs by boundary element method. Journal of Petroleum Science and Engineering 162, 84-101.
53. Xia, D., Yang, Z., Li, D., Zhang, Y., Zhao, X., Yao, L., (2021). Research on numerical method for evaluation of vertical well volume fracturing effect based on production data and well test data. Journal of Petroleum Exploration and Production 11, 1855-1863.
54. Xu, Y., Li, X., Lin, Q., Tan, X., (2021). Pressure performance of multi-stage fractured horizontal well considering stress sensitivity and dual permeability in fractured gas reservoir. Journal of Petroleum Science and Engineering 201, June, 108154.
55. Xue, Y., Jin, Q., Tian, H., (2021). Productivity Influence factors of tight sandstone gas reservoir with water produced. Geofluids Volume 2021, Article ID 9926299, 9 pages.
56. Yan, Z., Cao, C., Xie, M., Jia, P., Liu, G., Wei, X., Cheng, L., Tu, Z., (2021). Pressure behavior analysis of permeability changes due to sand production in offshore loose sandstone reservoirs using boundary-element method. Geofluids Volume 2021, Article ID 6658875, 10 pages.
57. Yang, Y., Peng, X., Liu, X., (2012). The stress sensitivity of coal bed methane wells and impact on production. Procedia Engineering 31, 571-579.
58. Yuan, B., Clarlson, C. R, Zhang, Z., Zhu, X., (2021). Deviation from transient linear flow behavior: A systematic investigation of possible control on abnormal reservoir signatures. Journal of Petroleum Science and Engineering 05, October 2021, 108910
59. Zhang, Y. G., Tong, D. K., (2008). The pressure transient analysis of deformation of fractal medium. Journal of Hydrodynamics 20(3), 306–313.
60. Zhang, L., Guo, J., Liu, Q., (2010). A well test model for stress-sensitive and heterogeneous reservoirs with non-uniform thicknesses. Pet. Sci. 7, 524-529.
61. Zhang, L.-H., Guo, J.-J., Liu, Q.-G.., (2011). A new well test model for stress-sensitive and radially heterogeneous dual-porosity reservpirs with non-uniform thicknesses. Journal of Hydrodynamics 23(6). 759-766.
62. Zhang, Z., He, S., Liu, G., Guo, X., Mo, S., (2014). Pressure buildup behavior of vertically fractured wells with stress-sensitive conductivity. Journal of Petroleum Science and Engineering 122, 48-55
63. Zhang, Z., He, S., Gu, D., Gai, S., Li, G., (2017). Effects of stress-dependent permeability on well performance of ultra-low permeability oil reservoir in China. J Petrol Explor Prod Technol 2017.
64. Zhang, J., Wei, C., Ju, W., Yan, G., Lu, G., Hou, X., Kai, Z., (2019). Stress sensitivity characterization and heterogeneous variation of the porefracture system in middle-high rank coals reservoir based on NMR experiments. Fuel 238, 331-344.
65. Zhang, Y., Yang, D., (2021)a. Modeling transient pressure behavior of a multi-fractured horizontal well in a reservoir with an arbitrary boundary and different fracture networks by considering stress-sensitive effect. Journal of Hydrology 600, September 2021, 126552.
66. Zhang, Y., Yang., D., (2021)b. Evaluation of transient pressure responses of a hydraulically fracture horizontal well in a tight reservoir with an arbitrary shape by considering stress-sensitive effect. Journal of Petroleum Science and Engineering 202, July 2021.
67. Zhao, L., Fan, Z., Wang, M., Xing, G., Zhao, W., Tan, C., Cheng, Y., (2020). Productivity evaluation of vertical wells incorporating fracture closure and reservoir pressure drop in fractured reservoirs. Mathematical Problems in Engineering 2020, Article ID 9356178, 11pages.
68. Zhao, C., Min, Ch., (2021). Analysis of the transient flow of non-Newtonian power-law fluids in homogeneous reservoirs with the elastic outer boundary. Acta Geophysica 69, 1865-1875.
69. Zheng, S., 2015. The Research on the pressure sensitivity for low permeability fractured CBM reservoir. International Journal of Earth Sciences and Engineering 8(2), 9-13.
70. Zheng, P., Zheng, Y., Li, S., Leng, L., Xia, X., (2021). Analysis of flow characteristics of the dual media shale gas reservoir with the elastic outer boundary. SN Applied Sciences (2021) 3:800.
71. Zhu, Q. and Liang, H., (2017). Productivity analysis method of abnormal high-pressure gas reservoir in Ying-Qiong Basin. Natural Resources 8, 410-415.
72. Zhu, H., Tang, X., Liu, Q., Liu, S., Zhang, B., Jiang, S., McLennan, J. D., (2018). Permeability stress-sensitivity in 4D flow-geomechanical coupling of Shouyang CBM reservoir, Qinshui Basin, China. Fuel 232, 817–832.
73. Zongxiao, R., Xiaodong, W., Guoqing, H., Lingyan, L., Xiaojun, W., Guanghui, Z., Hun, L., Jiaming, Z., Xianwei, Z., (2017). Transient pressure behavior of multi-stage fractured horizontal wells in stress-sensitive tight oil reservoirs. Journal of Petroleum Science and Engineering 157, 1197-1208.

DOI:10.31579/2690-1919/406